International Journal of Automotive and Mechanical Engineering (IJAME)
ISSN: 2229-8649 (Print); ISSN: 2180-1606 (Online)
Volume 12, pp. 2829-2843, July-December 2015

DOI: http://dx.doi.org/10.15282/ijame.12.2015.3.0238

Effect of ZnO nano materials on grinding surface finishing

M. Yogeswaran[1], K. Kadirgama[1,2]* , M.M. Rahman[1,2], R. Devarajan[1,2] and M.M. Noor[1,2]

[1]Faculty of Mechanical Engineering,
Universiti Malaysia Pahang, 26600 Pekan, Pahang, Malaysia
Email: kumaran@ump.edu.my
Phone: +6094246239; Fax: +6094246222

ABSTRACT

Surface roughness is a variable often used to describe the quality of ground surfaces as well as to evaluate the competitiveness of the overall grinding system. The subject of this paper is a grinding process performed on P20 tool steel by changing the grinding conditions, including the depth of cut, the grinding passes, the type of wheel, and the cutting fluid supply in the experiment. The main objective was to investigate the effect of ZnO nanofluid on the grinding surface finishing and wheel wear. The machined surface of selected specimens underwent SEM to assess the surface integrity. An artificial neural network was used to predict the surface roughness and recognize the trend of the surface roughness. The result showed the reduction of 47 % surface roughness value in grinding with ZnO nanofluid. The neural network made accurate predictions and could recognize the roughness trend.

Keywords: ZnO; grinding; surface roughness; P20 tool steel.

INTRODUCTION

Grinding is a finishing machine operation to ensure final surface quality. During the grinding process, small chips are removed along with large amounts of material. Since grinding is mostly used as a finishing method to determine the functional properties of the surface, knowledge of the surface quality and its control are crucial [1, 2]. It is therefore a challenge to achieve high levels of surface quality, conditionally improved by the grinding process, and choose the appropriate cutting conditions. The issue of wear has been addressed primarily for materials prone to high adhesion [3]. The chemical and metallurgical mechanisms of adhesion of metal to grit have been studied with a view to assessing the blunting and attrition of the wheel. In terms of surface damage it has been suggested that the adhered material acts as a tool of large nose radius to tear and plough out large grooves on the surface [4]. These modes are clearly sensitive to material properties such as hardness, toughness and fatigue strength, and their operative values are dependent on the strain, strain rate and temperature generated in the contact zone. As stated above, the localization of heat influenced by thermal conductivity of material is a factor which is likely to affect wear and surface roughness [5]. The latter authors addressed the issue of material response to grinding, in generating surface roughness.

Cutting fluid is a term generally used to describe fluids used for cooling and lubrication in grinding. The main purpose of a grinding fluid is to minimize mechanical, thermal, and chemical impact between the active partners of the abrasion process. The

lubricating effect of a grinding fluid reduces friction between the abrasive grains and the workpiece, as well as between the bond and the workpiece [6]. Nanofluids are a relatively new class of fluids and consist of a base fluid with nano-sized particles (1 to 100 nm) suspended within them. These particles, generally a metal or metal oxide, increase conduction and convection coefficients, allowing for more heat transfer out of the coolant [7-10]. These features make the nanofluid very attractive for cooling or lubricating applications in many industries including manufacturing, transportation, energy, and electronics [6]. Nanofluids are defined as suspended nanoparticles in a base fluid. Compared with conventional solid-liquid suspensions for heat transfer intensification, nanofluids possess advantages such as a high specific surface area [2, 11, 12] and therefore more heat transfer surface between particles and fluids, reduced particle clogging compared with conventional slurries, thus promoting system miniaturization, and adjustable properties, including thermal conductivity and surface wettability obtained by varying particle concentrations to suit different applications [6, 8, 13, 14].

Conventional heat conduction models for solid-liquid mixtures have long been established such as the Maxwell model [15], the Hamilton-Crosser model [16] and the Jeffrey model [17]. However, these conventional heat conduction models were confined to dispersions containing millimetre- or micrometer-sized particles. When applied to nanofluids, they usually underestimate the thermal conductivity [18-20]. Choi et al. [21] found that the effective thermal conductivity of ethylene glycol improved by up to 40% through the dispersion of 0.3 vol% Cu nanoparticles of 10 nm mean diameter, and Xuan and Li [22] demonstrated that the effective thermal conductivity of water increased by up to 78% with 7.5 vol% Cu nanoparticles of 100 nm mean diameter. Hong et al. [23] reported that the thermal conductivity of Fe nanofluids increased nonlinearly up to 18% as the volume fraction of particles increased up to 0.55 vol%. Patel et al.[24] studied the behavior of Au and Ag nanoparticles dispersed in water and found that water-soluble Au nanoparticles, 10 to 20 nm in mean diameter, derived from citrate stabilization showed thermal conductivity enhancement of 5 to 21% in the temperature range of 30 to 60ºC at a loading of 0.026 vol%. The early research work by Masuda et al. [25] reported 30% increases in the thermal conductivity of water with the addition of 4.3 vol% Al_2O_3 nanoparticles (average diameter of 13 nm). A subsequent study by Lee et al. [20], however, observed only a 15% enhancement in thermal conductivity at the same nanoparticle loading (average diameter of 33 nm). Xie et al. [26] found an intermediate result, that is, the thermal conductivity of water was enhanced by approximately 21% by a nanoparticle loading of 5 vol% (average diameter of 68 nm). These differences in behavior were attributed to differences in the average particle size of the samples. Nanofluids consisting of CuO nanoparticles dispersed in water and ethylene glycol seem to have larger enhancements in thermal conductivity than those containing Al_2O_3 nanoparticles [21]. The early research by Eastman et al. [21] showed that an increase in thermal conductivity of approximately 60% can be obtained for the nanofluid consisting of water and 5 vol% CuO nanoparticles with average grain size of 36 nm. Lee et al.[20] observed only a modest improvement of nanofluids containing CuO compared with those containing Al2O3, but Zhou and Wang [27] observed a 17% increase in thermal conductivity for a loading of only 0.4 vol% CuO nanoparticles in water. Xie et al. [28] studied SiC (average diameter of 26 nm) in water suspension and reported that the thermal conductivity could be increased by about 15.8% at 4.2 vol%. Murshed et al. [29] showed that the measured thermal conductivity for water-based TiO_2 nanofluids (average diameter of 15 nm) had a maximum enhancement of 30% for 5 vol% of particles.

The aim of this study is to investigate the performance of engineered nanofluid regarding the grinding process and the ability of neural networks to predict/recognize surface roughness.

EXPERIMENTAL SETUP

AISI P20 tool steel is a low carbon tool steel containing chromium and molybdenum alloying elements. The hardness of the AISI P20 tool steel has a Brinell hardness number of around 300. The ZnO nanofluid iwas prepared by a single-step dilute approach. ZnO nanofluid procured from SIGMA ALDRICH had 35wt % of nanoparticles of 100nm. The concentration of the nanofluid expressed in terms of volume percent ϕ is estimated with Eq. (1).

The expression for conversion of wt% φ to vol% ϕ is shown in Eq. (1):

$$\phi = \frac{\varphi\rho_w}{(1-\varphi)\rho_p + \varphi\rho_w} \tag{1}$$

where ϕ is the volume concentration of the nanofluid, φ is weight percentage of the nanoparticles, ρ_w is density of the distilled water, ρ_p is density of the nanoparticles.

The grinding processes were conducted by using two types of cutting fluid, water-based coolant and ZnO nanofluid. For the water-based coolant, two different types of wheel were used, Al_2O_3 and SiC wheels. For each type of wheel, the grinding processes were conducted in conditions of single-pass and multi-pass grinding. For each type of grinding setup, a different depth of cut was manipulated to investigate the relationship between depths of cut and surface roughness. The manipulated depths of cut for each grinding setup were 5 µm to 21 µm. The arithmetic surface roughness, Ra, was then measured on the ground area. The total number of grinding experiments was 54.

ARTIFICIAL NEURAL NETWORK

In the current application, the objective was to use the supervised network with multilayer perceptrons and train with the back-propagation algorithm (with momentum). The components of the input pattern consisted of the control variables used in the machining operation (depth of cut), whereas the components of the output pattern represented the responses from sensors (surface roughness). The nodes in the hidden layer were necessary to implement nonlinear mapping between the input and output patterns. During the training process, first all patterns in the training set were presented to the network and the corresponding error parameter (sum of squared errors over the neurons in the output layer) was found for each of them [30]. Subsequently, the pattern with the maximum error was obtained and used to change the synaptic weights. Once the weights were changed, all the training patterns were again fed into the network and the pattern with the maximum error was then found. This process continued until the maximum error in the training set was less than the allowable error specified by the user. This method has the advantage of avoiding a large number of computations, since only the pattern with the maximum error is used to change the weights [30-32]. First, a set of training data that consists of the normalized values of the input patterns and the corresponding output data is used to determine the connection weights.

Once the network is trained to such an extent that the maximum error of any training data is less than the allowable error, the weights and the threshold values are automatically saved by the program. As the input values from the validation experiments are given to the NN program, the program predicts the required output. The architecture transfer function of linear tanh axon and the learning rule function of online backpropagation were used for the output layer and hidden layers. The total number of epochs was 10000 and the MSE was 10^{-6} and was repeated for a higher number of neurons between 13 and 30 [33]. The heuristic method was used to find the best hidden layer with an evaluation of R2, as shown in Table 1. Three standard criteria R2, RMSE and MRE were selected to evaluate the various networks (R is the error, RMSE is the root mean square error, and MRE is the mean relative error) [30]. A regression analysis between the network response and corresponding targets was performed to investigate the network response in more detail. Different training algorithms were tested and online backpropagation was selected. Therefore, a network with one hidden layer and 17 neurons was selected as the preferred ANN.

Table 1. Heuristic search.

ID	Network	Fitness	Train Error	Validation Error	Test Error	Correlation	R-Squared
7	[1-17-1]	0.97889	0.685131	15.30876	3.041863	0.991344	0.97889
5	[1-7-1]	0.976284	0.797528	15.92875	4.81254	0.988432	0.976284
9	[1-8-1]	0.948303	1.065103	14.80459	3.110027	0.981339	0.948303
6	[1-4-1]	0.948258	1.093678	15.35659	4.67719	0.995869	0.948258
4	[1-11-1]	0.944728	1.065221	13.51954	2.117756	0.980786	0.944728
2	[1-30-1]	0.897942	1.432887	14.38161	2.947662	0.978286	0.897942
1	[1-1-1]	0.810318	2.012331	15.76841	6.931578	0.904002	0.810318
8	[1-10-1]	0.654642	2.667532	16.34068	9.145041	0.812542	0.654642
3	[1-18-1]	0.638024	2.701946	16.76851	9.617552	0.8018	0.638024

Table 2. Summary of the training.

	Target	Output	Absolute Error	Absolute Relative Error
Mean	33	33.04806	0.062858	0.002126
Standard deviation	5.24404	5.199577	0.033662	0.001404
Min	26	26.10577	0.029605	0.000777
Max	39	39.03029	0.105766	0.004068

Table 3. Summary of the overall network.

	Target	Output	Absolute Error	Absolute Relative Error
Mean	38.8333	37.05355	1.853722	0.034803
Standard deviation	9.82203	7.130522	3.434434	0.060891
Min	26	26.10577	0.029605	0.000777
Max	56	46.54702	9.452984	0.168803

An independent ANN test was conducted for a specific range of depth of cut for different parameters to establish confidence in the ANN model. Initial tests were conducted to predict the relationship between the depth of cut and surface roughness [25]. The training summary is shown in Table 2. The R2 is 0.9771 and correlation is 0.9784. The overall summary is shown in Table 3. The R2 is 0.9811 and correlation 0.9834.

RESULTS AND DISCUSSION

Single-Pass Experiment

Figure 1 shows the variation of surface roughness with different depth of cut for the single-pass experiment. Generally, the trend of the surface roughness, Ra, increases constantly when the depth of cut increases. The silicon carbide wheel obtained the highest value of surface roughness, which was 0.710µm for a cutting depth of 5µm. However, the surface roughness increased inconstantly until 1.748µm for a cutting depth of 21µm. On the other hand, the experiment which was conducted with a water-based coolant with an aluminum oxide wheel obtained a surface roughness slightly lower than in the first experiment. The surface roughness for a 5µm cutting depth was 0.622µm and it increased constantly until 1.687µm. The experiment conducted using zinc oxide nano-coolant obtained the lowest value of surface roughness, which was 0.446µm for a cutting depth of 5µm, and it increased to 1.120µm for a cutting depth of 21µm. In general, the measurements of surface roughness showed an increase in magnitude as the depth of cut increased. This is because the heat generation between the work piece and grinding tool zone was higher for the greater depths of cut. The higher heat generation in this zone contributed to the burning effect on the workpiece. Therefore, the higher the axial depth of the cut, the higher the surface roughness [6]. For lower cutting depth, more grains participated in material removal and hence the depth of engagement was lower and produced smooth surfaces. However, for higher cutting depth the grain that interacted with the workpiece perform the undeformed chip on the work piece surface which produces a rough surface [6, 34]. Hence, the surface roughness increases when the depth of cut increases in grinding machinability.

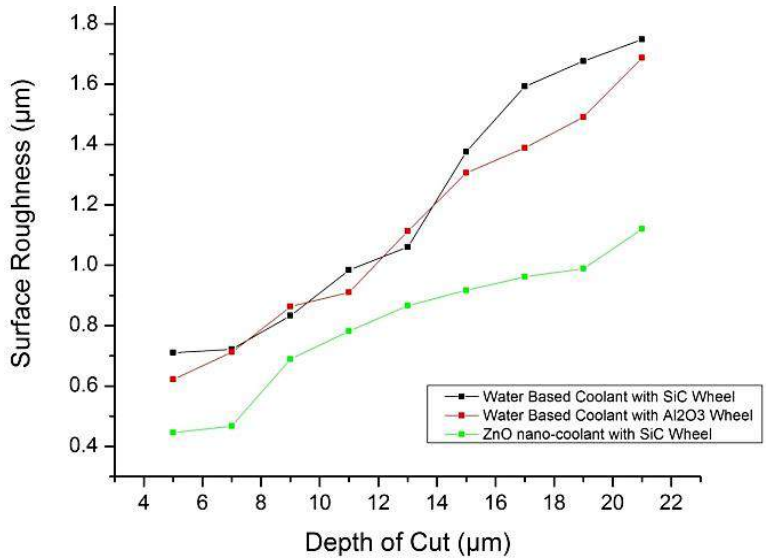

Figure 1. Surface roughness versus depth of cut for single-pass grinding.

The experiment conducted using water-based coolant with an aluminum oxide wheel obtained lower surface roughness, Ra, compared with that conducted with the silicon carbide wheel. This is because of the different hardness of the wheels. Therefore, in a single-pass experiment with a silicon carbide wheel, first the grinding wheel grinds in the self-sharpening region where bond post fracture is predominant and later grinds in a zone of mixed conditions; for example, partly sharpening and partly blunting. In the

final range blunting becomes predominant [27]. This proves that workpieces ground with a silicon carbide wheel have high surface roughness compared with those ground with an aluminum oxide wheel. The experiment conducted using a zinc oxide nano-coolant obtained the lowest surface roughness, Ra. This is because zinc oxide nano-coolant has high thermal conductivity compared with water-based coolants. Therefore, nano-coolant has the ability to carry away the heat in the grinding zone [27]. Once the heat has been removed from the grinding zone, the burning defect does not appear on the surface of the workpiece. Therefore the surface roughness, Ra, of the workpiece is much higher than that provided by the water-based coolant.

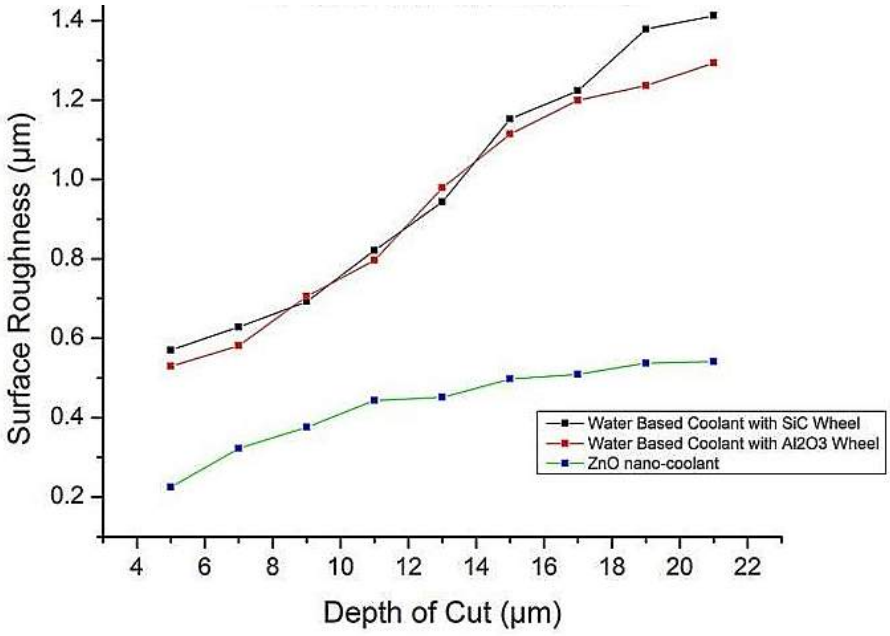

Figure 2. Surface roughness versus depth of cut for multi-pass grinding.

Multi-Pass Experiment

Figure 2 shows the variation of surface roughness with different depths of cut for the multi-pass experiment. Generally, the trend of the surface roughness, Ra, increases inconstantly when the depth of cut increases. First, the experiment conducted with water-based coolant and a silicon carbide wheel obtained the highest value of surface roughness, Ra, which was 0.570μm for a cutting depth of 5μm. However, the surface roughness, Ra, increased inconstantly until 1.412μm for a cutting depth of 21μm. On the other hand, the experiment conducted with water-based coolant and an aluminum oxide wheel obtained slightly lower surface roughness than the first experiment. The surface roughness, Ra, for a 5μm cutting depth was 0.529μm and it increased inconstantly until 1.293μm. However, the experiment was conducted using a zinc oxide nano-coolant which obtained the lowest value of surface roughness, Ra, which was 0.225μm for a cutting depth of 5μm and increased to 0.541μm for a cutting depth of 21μm. As stated above, the reason for the trend of the graph for the multi-pass experiment is similar to that for the single-pass experiment. However, the surface roughness, Ra, result obtained for the former is lower than for the latter. This is because when the single-pass grinding experiment is conducted on the surface of the workpiece, the grain engages with the workpiece in up-cut grinding, and slides without cutting the workpiece surface because of the elastic deformation of the system. In the multi-pass grinding experiment, however, the workpiece material piles up

at the front and sides of the grain to form a groove and complete chips are performed [18]. Therefore, the multi-pass grinding experiment obtained a better surface roughness, Ra, than the single-pass grinding experiment.

Metallographic Analysis of Water-Based Coolant

Figure 3 shows the SEM results for experiments conducted using water-based coolant for a cutting depth of 5 µm. It can be seen in Figure 3(b) that there are little burnt areas on the workpiece surface. There are also some continuous smooth scratches on the grind surface. These scratches were produced by the interactions of abrasive cutting points with the workpiece. Since the interactions between the points and the workpiece were few for a cutting depth of 5 µm, the scratches are finer. On the other hand, the grinding grooves are almost the same in width and depth. In previous research, when the interface temperature was high enough, the workpiece material at the contact zone became ductile enough to cause strong welds to form between the abrasive grit and the workpiece, thereby resulting in the generation of plastically deformed coatings [26]. This supports the appearance of some burn-colored scratches on the workpiece surface.

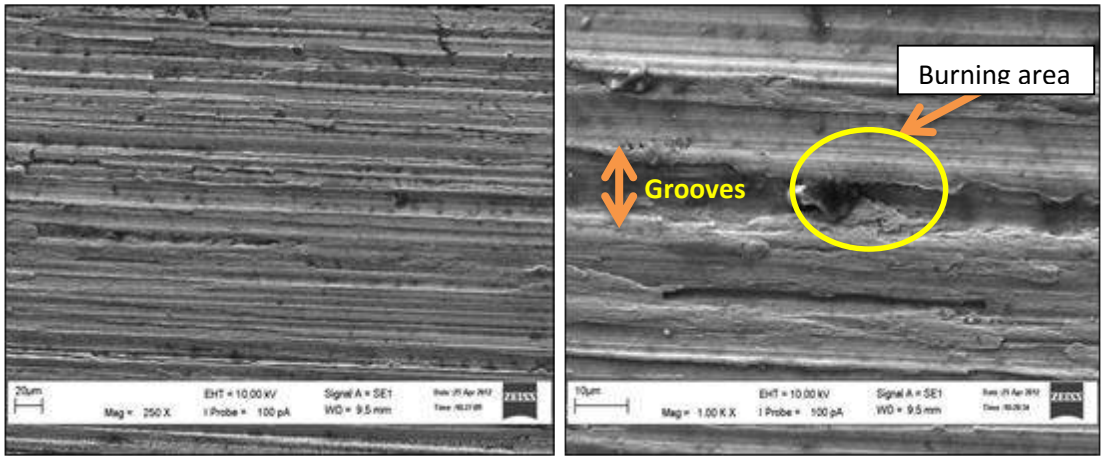

(a) Magnification of 250x (b) Magnification of 1000x

Figure 3. SEM result for a cutting depth of 5µm.

Figure 4 shows the SEM results for experiments conducted using water-based coolant for a cutting depth of 11 µm. Figure 4(b) shows a lot of burn-colored marks on the workpiece surface compared with Figure 3(b). The groove size is unequal in width and depth. There are also many more overlapping scratches compared with Figure 3(b). This is because when cutting depth is increased the heat generated in the grinding zone is higher. Therefore, the possibility of burns on the workpiece surface is higher. As stated before, when the grinding interface temperature is high enough, the workpiece material at the contact zone becomes ductile enough to cause strong welds to form between the abrasive grit and the workpiece, thereby resulting in the generation of plastically deformed coatings [26].

Figure 5 shows the SEM results for experiments conducted using water-based coolant for a cutting depth of 21µm. In Figure 5(b) there are a lot of large burn marks on the workpiece surface compared with Figures 3(b) and 4(b). The scratches produced by a cutting depth of 21µm also overlap each other. Furthermore, the grooves are unequal and not continuous. On the othe hand, there are a lot of raised edges or small pieces of material

which remain attached to the workpiece; these are known as burrs on the surface. This contributes to a high value of surface roughness. It happens because of the plastic deformation on the surface of the material in conjunction with the thermal effect [35]. Also,the excessive heat penetrates the workpiece and contributes to the huge amount of burning on the workpiece surface.

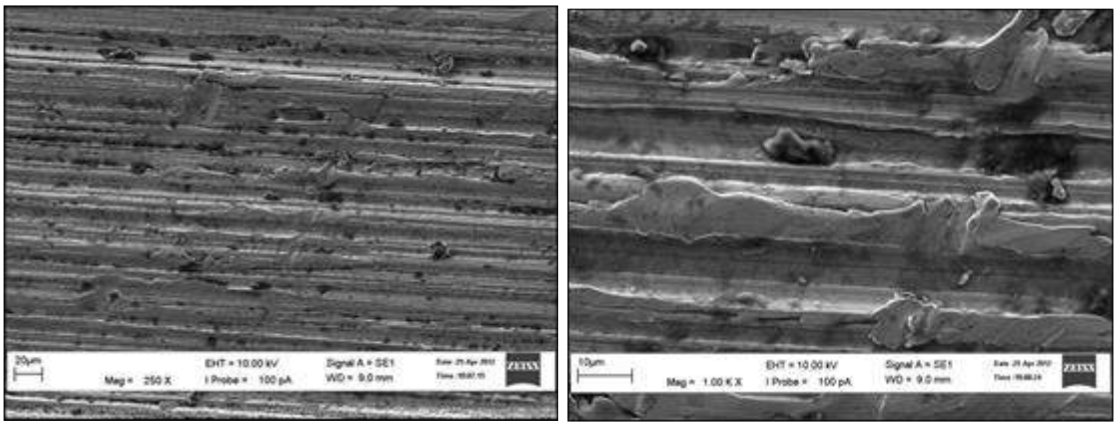

(a) Magnification of 250x (b) Magnification of 1000x

Figure 4. SEM result for a cutting depth of 11µm.

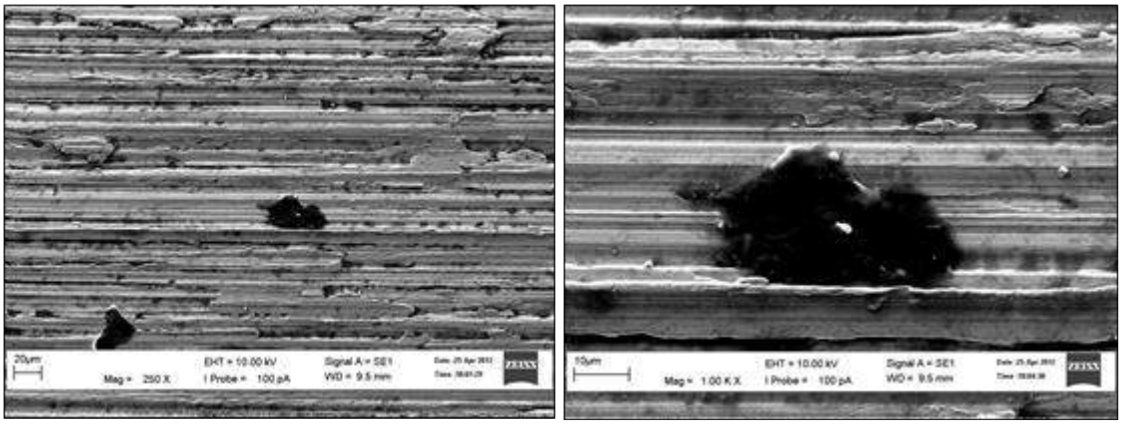

(a) Magnification of 250x (b) Magnification of 1000x

Figure 5. SEM result for a cutting depth of 21 µm.

Metallographic Analysis of Zinc Oxide Nano-Coolant

Figure 6 shows the SEM results for experiments conducted using zinc oxide nano-coolant for a cutting depth of 5µm. In Figure 6(a) there are fewer burn marks on the workpiece surface compared with Figures 3(b) and 4(b) and scractches produced are very smooth compared with Figures 3(b) and 4(b). Furthermore, the grooves in the finished surface after grinding with zinc oxide nano-coolant are smoother, wider and shallower than with water-based coolant. No burrs occurred on this surface. The finest surface roughness is achieved compared with the other experiment because of the high thermal conductivity of zinc oxide nano-coolant which absorbs the heat that penetrates the workpiece during grinding. This phenomenon causes less burning and less plastic deformation than when water-based coolant is sused. On the other hand, zinc oxide nano-coolant's high viscosity

reduces the sliding friction between the wheel and workpiece [6]. Reduction in sliding friction produces the smooth grooves on the workpiece surface shown in Figure 6.

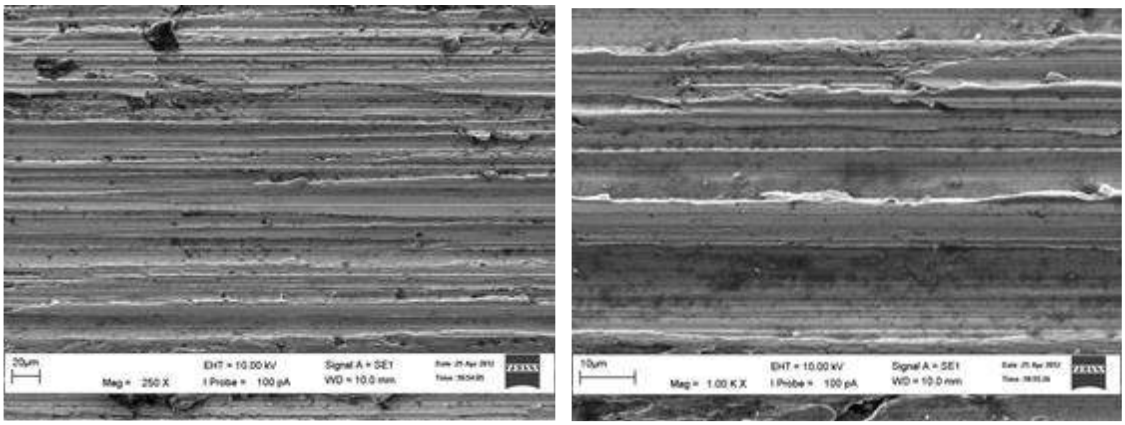

(a) Magnification of 250x (b) Magnification of 1000x

Figure 6. SEM result for a cutting depth of 5µm.

Figure 7 shows the SEM results for experiments conducted using zinc oxide nano-coolant for a cutting depth of 11µm. The results show that the scratches produced are rough compared with those in Figure 7(a). Moreover, the grooves are inconsistent in size. There are some grooves that are wide and deep. There are also some grooves that are very shallow. However, compared with Figure 3(b) which used water-based coolant for a cutting depth of 11µm, this experiment produced many more fine scratches and grooves. This is because the zinc oxide nano-coolant carries away the heat generated in the grinding zone [27].Therefore, there are fewer plastic deformations on the material surface and a better surface roughness is produced.

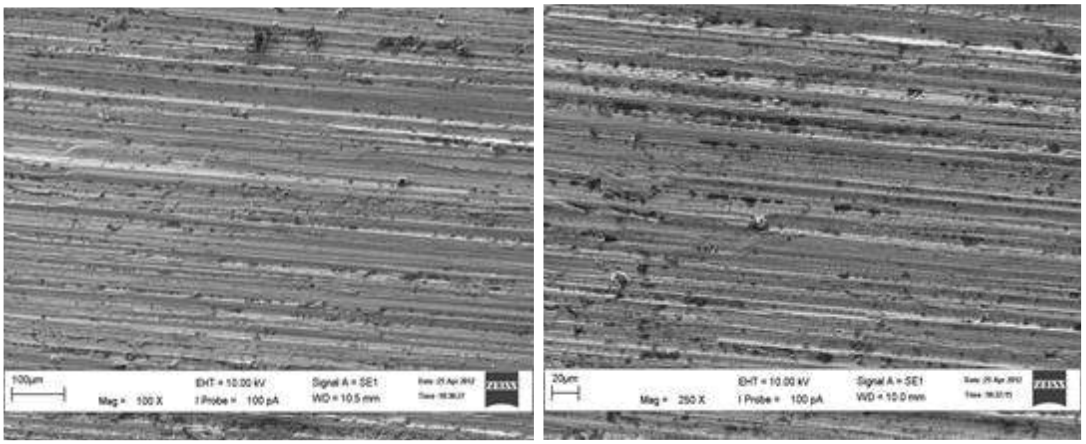

(a) Magnification of 250x (b) Magnification of 1000x

Figure 7. SEM result for a cutting depth of 11µm.

Figure 8 shows the SEM results for experiments conducted using zinc oxide nano-coolant for a cutting depth of 21µm. The results show that the scratches produced are very rough compared with those in Figure 7(b). In addition, the grooves are unequal and not

continuous, but there are fewer burrs than in Figure 7(b). This shows that there is some improvement on the surface microstructure when a zinc oxide nano-coolant is used. As stated before, this is owed to the high thermal conductivity of the nano-coolant. Nanoparticles tend to carry away the heat generated in the grinding zone [6]. However, the heat generated in the grinding zone for a cutting depth of 21µm are much higher than for cutting depths of 5µm and 11µm.

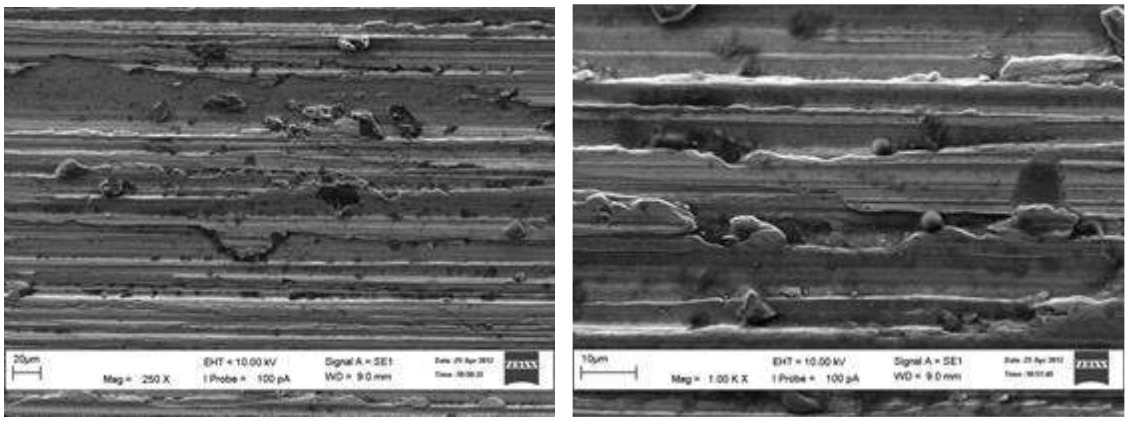

(a) Magnification of 250x (b) Magnification of 1000x

Figure 8. SEM result for a cutting depth of 21µm.

Analysis of Wheel Wear

Figure 9 shows the variation of wheel wear with different cutting depths using water-based coolants and zinc oxide nano-coolant for grinding. Generally, the graph trend of wheel wear increases inconstantly when the depth of cut increases for water-based coolant grinding. No experiments obtained any wheel wear for a cutting depth of 5µm. The multi-pass grinding using water-based coolant had the highest wheel wear compared with other experiments; it increased to 0.10 mm for a cutting depth of 21µm. However, the same experiment conducted with single-pass grinding resulted in slightly less wear. For a cutting depth of 21µm, the wheel wear was 0.08mm. Overall, the wheel wear increases when there is an increase in cutting depth of the grinding for water-based coolant grinding. This is because an increase in the depth of cut contributes to a rapid increase in normal force on the grinding wheel. Therefore the wheel fails to remove all the metal that is fed to it. Consequently, the down feed becomes interference and causes a rapid increase of the normal force and grinding becomes progressively less efficient and increases the wheel wear [6, 27]. Figure 9 also shows that experiments conducted using multi-pass grinding obtain a high value of wheel wear compared with experiments conducted with single-pass grinding. This is because, in single-pass grinding, there are only grain fractures, which occur on the wheel, but bond fracture starts to occur in multi-pass grinding which contribute to dulling the wheel and increase the wheel wear [18]. For multi-pass grinding, this contributes to higher wheel wear. Figure 9 shows there is no significant change in the wheel wear with zinc oxide nano-coolant. This shows that zinc oxide nano-coolant is better protection against wheel wear because of the thin slurry layer on the wheel which protects the bonding material from thermal mechanical damage, thereby causing insignificant wear [6].

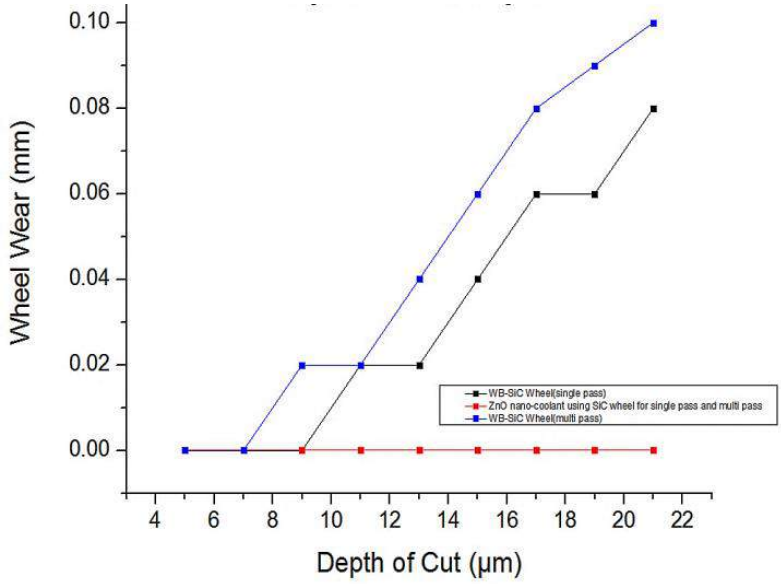

Figure 9. Wheel wear versus depth of cut for water-based coolant grinding.

Prediction Modeling of Artificial Neural Network

Figure 10 shows a prediction modeling graph using a neural artificial network for surface roughness versus depth of cut for single-pass grinding. Table 4 shows the prediction for grinding with water-based coolant with a silicon carbide wheel, which obtained the highest correlation between target and output of 0.996029. The R-squared is 0.929258. This figure shows there are strong relationships between the target and the output graph. Table 5 shows the prediction for grinding using a water-based coolant with an aluminum oxide wheel, which obtained a high correlation between the target and the output of 0.992852. The R-squared is 0.985055. There are strong relationships between the target and the output graph. Table 6 shows the prediction for grinding using zinc oxide coolant with a silicon carbide wheel, which obtained the lowest correlation between the target and output of 0.966179. The R-squared is 0.894227 [30, 31]. This shows there are strong relationships between the target and the output graph.

Table 4. Summary of predictions for water-based coolant with SiC wheel grinding.

	Target	Output	Absolute Error	Relative Error
Mean	1.189	1.198313	0.073789	0.071605
Standard Deviation	0.391572	0.31454	0.039421	0.052525
Minimum Value	0.71	0.816886	0.000037	0.000037
Maximum Value	1.748	1.635559	0.11893	0.164723
Correlation			0.996029	
R-squared			0.929258	

Table 5. Summary of predictions for water-based coolant with Al_2O_3 wheel grinding.

	Target	Output	Absolute Error	Relative Error
Mean	1.121444	1.125834	0.03617	0.033075

Standard Deviation	0.348127	0.342651	0.021128	0.020827
Minimum Value	0.622	0.659391	2.09×10^{-8}	2.94×10^{-8}
Maximum Value	1.687	1.625016	0.061984	0.060114
Correlation			0.992852	
R-squared			0.985055	

Table 6. Summary of predictions for zinc oxide nano-coolant with SiC wheel grinding.

	Target	Output	Absolute Error	Relative Error
Mean	0.804222	0.796192	0.05228	0.079059
Standard Deviation	0.218861	0.188716	0.032153	0.062284
Minimum Value	0.446	0.521369	0.003666	0.003998
Maximum Value	1.12	1.025737	0.094263	0.185242
Correlation			0.966179	
R-squared			0.894227	

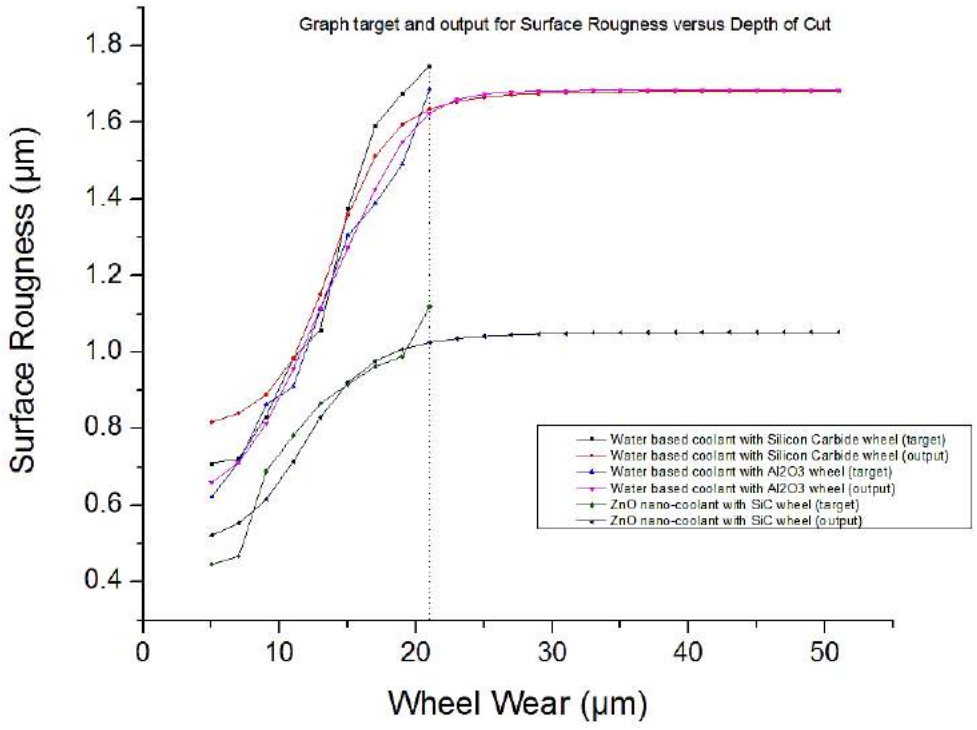

Figure 10. Artificial neural network prediction for single-pass grinding.

CONCLUSIONS

These conclusions are drawn from the analysis of single-pass and multi-pass grinding experiments using SiC wheel and an Al_2O_3 wheel with water-based coolant and TiO_2 nanofluid as cutting fluids. It can be concluded that the increments of the axial depth of cut increased the surface roughness of the grounded area. The surface roughness value is directly proportional to the depth of cut. The result indicates that better surface quality of the workpiece can be obtained at a lower depth of cut. Moreover, grinding with TiO_2 nanofluid produces better grinding surface quality than grinding with water-based

coolant. The reduction in surface roughness was observed to be from 20% to 40% in grinding condition with TiO_2 nanofluid as the cutting fluid. An artificial neural network predicted the roughness accurately and recognized the pattern of roughness.

ACKNOWLEEDGMENT

Author would like to thanks Universiti Malaysia Pahang for providing grant under RDU110373 to conduct the research.

REFERENCES

[1] Sahid NSM, Rahman MM, Kadirgama K. Neural Network Modeling of Grinding Parameters of Ductile Cast Iron Using Minimum Quantity Lubrication. International Journal of Automotive and Mechanical Engineering. 2015;11:2608-21.

[2] Rahman MM, Kadirgama K, Ab Aziz AS. Artificial neural network modeling of grinding of ductile cast iron using water based SiO_2 nanocoolant. International Journal of Automotive and Mechanical Engineering. 2014;9:1649-61.

[3] Sámek D, Bílek O, Cerny J. Prediction of grinding parameters for plastics by artificial neural networks. International Journal of Mechanics. 2011;5:250-61.

[4] Kadirgama K, Noor MM, Rahman MM. Optimization of Surface roughness in end milling using potential support vector machine. Arabian Journal for Science and Engineering. 2012;37:2269-75.

[5] Kadirgama K, Abou-El-Hossein KA, Noor MM, Sharma KV, Mohammad B. Tool life and wear mechanism when machining Hastelloy C-22HS. Wear. 2011;270:258-68.

[6] Shen B, Shih AJ, Tung SC. Application of nanofluids in minimum quantity lubrication grinding. Tribology Transactions. 2008;51:730-7.

[7] Hussein AM, Bakar RA, Kadirgama K. Study of forced convection nanofluid heat transfer in the automotive cooling system. Case Studies in Thermal Engineering. 2014;2:50-61.

[8] Rao GS, Sharma KV, Chary SP, Bakar RA, Rahman MM, Kadirgama K, et al. Experimental study on heat transfer coefficient and friction factor of Al_2O_3 nanofluid in A Packed bed column. Journal of Mechanical Engineering and Sciences. 2011;1:1-15.

[9] Mahendran M, Lee GC, Sharma KV, Shahrani A. Performance of Evacuated tube solar collector using water-based titanium oxide nanofluid. Journal of Mechanical Engineering and Sciences. 2012;3:301-10.

[10] Abdul Hamid K, Azmi WH, Mamat R, Usri NA, Najafi G. Effect of temperature on heat transfer coefficient of titanium dioxide in ethylene glycol-based nanofluid. Journal of Mechanical Engineering and Sciences. 2015;8:1367-75.

[11] Suriati G, Mariatti M, Azizan A. synthesis of silver nanoparticles by chemical reduction method: Effect of reducing agent and surfactant concentration. International Journal of Automotive and Mechanical Engineering. 2014;10:1920-7.

[12] Ravisankar B, Tara Chand V. Influence of nanoparticle volume fraction, particle size and temperature on thermal conductivity and viscosity of nanofluids- A review. International Journal of Automotive and Mechanical Engineering. 2013;8:1316-38.

[13] Hussein AM, Sharma KV, Bakar RA, Kadirgama K. Heat transfer enhancement with nanofluids – A review. Journal of Mechanical Engineering and Sciences. 2013;4:452-61.
[14] Azmi WH, Sharma KV, Mamat R, Anuar S. Nanofluid Properties for forced convection heat transfer: An overview. Journal of Mechanical Engineering and Sciences. 2013;4:397-408.
[15] Maxwell JC. An elementary treatise on electricity: Courier Dover Publications; 2005.
[16] Hamilton R, Crosser O. Thermal conductivity of heterogeneous two-component systems. Industrial & Engineering Chemistry Fundamentals. 1962;1:187-91.
[17] Jeffrey DJ. Conduction through a random suspension of spheres. Proceedings of the Royal Society of London A Mathematical and Physical Sciences. 1973;335:355-67.
[18] Chen X, Rowe WB. Analysis and simulation of the grinding process. Part I: generation of the grinding wheel surface. International Journal of Machine Tools and Manufacture. 1996;36:871-82.
[19] Jang SP, Choi SU. Effects of various parameters on nanofluid thermal conductivity. Journal of Heat Transfer. 2007;129:617-23.
[20] Lee S, Choi S-S, Li S, and, Eastman J. Measuring thermal conductivity of fluids containing oxide nanoparticles. Journal of Heat Transfer. 1999;121:280-9.
[21] Eastman J, Choi S, Li S, Yu W, Thompson L. Anomalously increased effective thermal conductivities of ethylene glycol-based nanofluids containing copper nanoparticles. Applied Physics Letters. 2001;78:718-20.
[22] Xuan Y, Li Q. Investigation on convective heat transfer and flow features of nanofluids. Journal of Heat Transfer. 2003;125:151-5.
[23] Hong T-K, Yang H-S, Choi C. Study of the enhanced thermal conductivity of Fe nanofluids. Journal of Applied Physics. 2005;97:064311.
[24] Patel HE, Das SK, Sundararajan T, Nair AS, George B, Pradeep T. Thermal conductivities of naked and monolayer protected metal nanoparticle based nanofluids: Manifestation of anomalous enhancement and chemical effects. Applied Physics Letters 2003;83:2931-3.
[25] Masuda H, Ebata A, Teramae K, Hishinuma N. Alteration of thermal conductivity and viscosity of liquid by dispersing ultra-fine particles. Netsu Bussei. 1993;7:227-33.
[26] Xie H, Wang J, Xi T, Liu Y, Ai F, Wu Q. Thermal conductivity enhancement of suspensions containing nanosized alumina particles. J Appl Phys. 2002;91:4568-72.
[27] Saidur R, Leong K, Mohammad H. A review on applications and challenges of nanofluids. Renewable and Sustainable Energy Reviews. 2011;15:1646-68.
[28] Xie G, Huang H. An experimental investigation of temperature in high speed deep grinding of partially stabilized zirconia. International Journal of Machine Tools and Manufacture. 2008;48:1562-8.
[29] Murshed S, Leong K, Yang C. Enhanced thermal conductivity of TiO_2—water based nanofluids. International Journal of Thermal Sciences. 2005;44:367-73.
[30] Khan MAR, Rahman MM, Kadirgama K, Maleque MA, Bakar RA. Artificial intelligence model to predict surface roughness of Ti-15-3 Alloy in EDM process. World Academy of Science, Engineering and Technology. 2011;50:194-8.
[31] Khan MAR, Rahman MM, Kadirgama K, Bakar RA. Artificial neural network model for material removal rate of TI-15-3 in electrical discharge machining.

Energy Education Science and Technology Part A: Energy Science and Research. 2012;29:1025-38.

[32] Khan MAR, Rahman MM, Kadirgama K, Maleque MA, Bakar RA. Artificial intelligence model to predict surface roughness of Ti-15-3 alloy in EDM process. World Academy of Science, Engineering and Technology. 2011;74:198-202.

[33] Rahman MM, Kadirgama K, Ab Aziz AS. Artificial neural network modeling of grinding of ductile cast iron using water based SiO_2 nanocoolant. International Journal of Automotive and Mechanical Engineering. 2014;9:1649-61.

[34] Liang SY, Hecker RL, Landers RG. Machining process monitoring and control: The state–of–the–art. ASME 2002 International Mechanical Engineering Congress and Exposition: American Society of Mechanical Engineers; 2002. p. 599-610.

[35] Maranhão C, Paulo Davim J. Finite element modelling of machining of AISI 316 steel: numerical simulation and experimental validation. Simulation Modelling Practice and Theory. 2010;18:139-56.